Theoretical band structure of the superconducting antiperovskite oxide $Sr_{3-x}SnO$

Atsutoshi Ikeda[a,*], Toshiyuki Fukumoto[b], Mohamed Oudah[a], Jan Niklas Hausmann[a,c], Shingo Yonezawa[a], Shingo Kobayashi[b,d], Masatoshi Sato[e], Cedric Tassel[f], Fumitaka Takeiri[f], Hiroshi Takatsu[f], Hiroshi Kageyama[f], Yoshiteru Maeno[a]

[a] *Department of Physics, Graduate School of Science, Kyoto University, Kyoto 606-8502, Japan*
[b] *Department of Applied Physics, Graduate School of Engineering, Nagoya University, Nagoya 464-8603, Japan*
[c] *Department of Chemistry, Faculty of Mathematics and Natural Sciences, Humboldt-Universität zu Berlin, Brook-Taylor-Strasse 2, Berlin 12489, Germany*
[d] *Institute for Advanced Research, Nagoya University, Nagoya 464-8601, Japan*
[e] *Yukawa Institute for Theoretical Physics, Kyoto University, Kyoto 606-8502, Japan*
[f] *Department of Energy and Hydrocarbon Chemistry, Graduate School of Engineering, Kyoto University, Kyoto 615-8510, Japan*

Abstract

In order to investigate the position of the strontium deficiency in superconductive $Sr_{3-x}SnO$, we synthesized and measured X-ray-diffraction patterns of $Sr_{3-x}SnO$ ($x \sim 0.5$). Because no clear peaks originating from superstructures were observed, strontium deficiency is most likely to be randomly distributed. We also performed first-principles band-structure calculations on $Sr_{3-x}SnO$ ($x = 0, 0.5$) using two methods: full-potential linearized-augmented plane-wave plus local orbitals method and the Korringa-Kohn-Rostoker Green function method combined with the coherent potential approximation. We revealed that the Fermi energy of $Sr_{3-x}SnO$ in case of $x \sim 0.5$ is about 0.8 eV below the original Fermi energy of the stoichiometric Sr_3SnO, where the mixing of the valence p and conduction d orbitals are considered to be small.

Keywords: superconductivity, antiperovskite oxide, inverse perovskite oxide, first-principles band calculation

1. Introduction

Antiperovskite (inverse perovskite) oxides A_3BO are the metal-rich counterparts of the ordinary perovskite oxides with the inverted metal and oxygen positions as schematically shown in Fig. 1(a). While in an ordinary perovskite oxide the metal elements at the unit-cell center are octahedrally surrounded by oxygens, in an antiperovskite oxide the oxygen atom is octahedrally coordinated by metal elements. The space group of antiperovskite oxides is basically the same as that of the ordinary cubic perovskite oxides ($Pm\bar{3}m$, No. 221, O_h^1) [1]. When A is a group-2 element and B is tin or lead, the oxidation state of B becomes 4− to satisfy the charge neutrality condition. Such a negative-ionic state of a metallic element is rare.

Some members of the antiperovskite oxides are actively studied in recent years for their non-trivial electronic structures. M. Klintenberg *et al.* reported a number of compounds including antiperovskite oxides with the inversions of the valence and conduction bands using a data-mining algorithm [4]. In 2011, T. Kariyado and M. Ogata found a linear dispersion in the band structure of some antiperovskite oxides such as Ca_3PbO and pointed out using a tight-binding model that the linear dispersion is a Dirac cone protected by the p-d band inversion and crystalline symmetry [5]. T. Kariyado and M. Ogata also indicated that the Dirac cone has a slight but nonzero band gap because of the higher-order effect of the spin-orbit coupling [6]. Later in 2014, T. H. Hsieh *et al.* theoretically revealed that the antiperovskite oxides with the band inversion and the gap opening are topological crystalline insulators [7]. Because of these theoretical proposals, antiperovskite oxides have been attracting experimentalists' interest [8, 9, 10, 11, 12].

Recently, a part of the present authors discovered that the hole-doped antiperovskite oxide $Sr_{3-x}SnO$ ($x \sim 0.5$) exhibits superconductivity, the first superconductivity among the antiperovskite oxides [13]. In a *moderately* hole-doped $Sr_{3-x}SnO$ with a rigid-band shift, reflecting the unusual topology of the normal state, possibility of the topological crystalline superconductivity due to the strong p-d mixing of the orbitals has been theoretically proposed. However, the actual band structure of the superconductive $Sr_{3-x}SnO$, as well as the distribution of the strontium deficiency in the crystal structure, has not been clear. In this paper, we present synchrotron powder X-ray diffraction spectra and the first-principles band-structure calculations on $Sr_{3-x}SnO$ ($x \sim 0.5$).

*Corresponding author
Email address: a.ikeda@scphys.kyoto-u.ac.jp (Atsutoshi Ikeda)

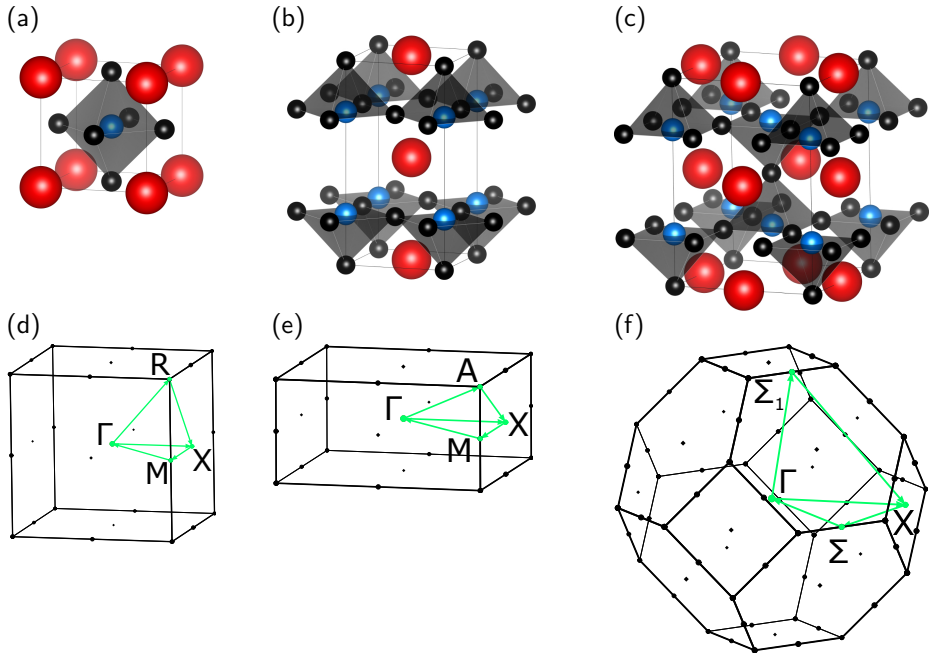

Figure 1: (a) Crystal structure of Sr_3SnO. The black, red, and blue spheres represent the strontium, tin, and oxygen atoms, respectively. The space group is $Pm\bar{3}m$ (No. 221, O_h^1). (b, c) Hypothetical structures of strontium-deficient $Sr_{3-x}SnO$ ($x = 0.5$). The structure (b) has the layers of the strontium deficiency resulting in a simple tetragonal lattice with the space group $P4/mmm$ (No. 124, D_{4h}^1). On the other hand, in the structure (c), the strontium atoms are vacant alternatively from different layers, resulting in a body-centered tetragonal lattice with the space group $I4/mmm$ (No. 139, D_{4h}^{17}). The figures of the crystal structures were prepared with the program VESTA [2]. Brillouin zones of the (d) simple cubic, (e) simple tetragonal, and (f) body-centered tetragonal lattices. The k paths for the band-structure plots in Figs. 3 and 4 are Γ-X-M-Γ-R-X for (d), Γ-X-M-Γ-A-X for (e), and Γ-X-Σ-Γ-Σ_1-X for (f). The figures of the Brillouin zones were drawn with the program XCrySDen [3].

2. Methods

Sample synthesis. Polycrystalline samples of $Sr_{3-x}SnO$ ($x \sim 0.5$) were synthesized by using the reaction:

$$(3 - x)\mathrm{Sr} + \mathrm{SnO} \rightarrow \mathrm{Sr}_{3-x}\mathrm{SnO}. \quad (1)$$

Strontium (Sigma-Aldrich Co. LLC., 99.99%) and tin(II) oxide (Furuuchi Chemical Corporation, 99.9%) were mixed in the molar ratio of 2.5:1 in an alumina crucible, and the crucible was sealed inside a quartz tube under 0.3 atm of argon at room temperature. The tubes were heated to 825°C over three hours, kept at 825°C for three hours, and then quenched in water [13]. A piece of chunk from this batch was confirmed to exhibit superconductivity below 5.2 K based on magnetization measurement.

Sample characterization. Powder-X-ray-diffraction measurement down to 30 K was performed at the beamline BL02B2 of the synchrotron facility SPring-8. The wavelength of the incident beam was $\lambda = 0.042073$ nm. Sample powder was sealed in a quartz tube under nitrogen to prevent decomposition of the air-sensitive $Sr_{3-x}SnO$ samples.

First-principles calculation. In order to investigate the actual band structure of $Sr_{3-x}SnO$, we performed first-principles calculations of the stoichiometric and deficient $Sr_{3-x}SnO$ with two programs: WIEN2k [14], which uses full-potential linearized-augmented plane-wave plus local orbitals method, and AkaiKKR (also called Machikaneyama) [15], using the Korringa-Kohn-Rostoker Green function method [16, 17]. In both packages, we used the Perdew-Burke-Ernzerhof generalized gradient approximation [18] as the exchange-correlation functional and took the spin-orbit coupling into account. We assumed paramagnetic states for both Sr_3SnO and $Sr_{3-x}SnO$ and did not perform spin-polarized calculations. The experimentally reported crystalline structure [11] was used for the calculation of Sr_3SnO. Figure 1(d) shows the Brillouin zone of the simple cubic lattice and k path used for the band-structure plot.

In the case of WIEN2k, the radius R of the muffin-tin sphere of each atom was set to $R_{\mathrm{Sr}} = R_{\mathrm{O}} = 2.39$ bohr and $R_{\mathrm{Sn}} = 2.5$ bohr. We set the plane-wave cut off $RK_{\max} = 7$, the highest angular momentum plus one $l_{\max} = 10$, maximum magnitude of the largest vector in charge density Fourier expansion $G_{\max} = 12$, and separation energy between the valence and core states -6.0 Ry. To see the effect of the strontium deficiency, we tried calculation on two hypothetical superstructures of $Sr_{3-x}SnO$ with different patterns of the deficiency, shown in Figs. 1(b) and (c). In the structure shown in Fig. 1(b), strontium atoms in certain layers are missing. In the structure of Fig. 1(c), strontium atoms are taken away alternatively from two neighboring layers. k meshes of $10\times10\times10$ were used for the calculation of Sr_3SnO and the body-

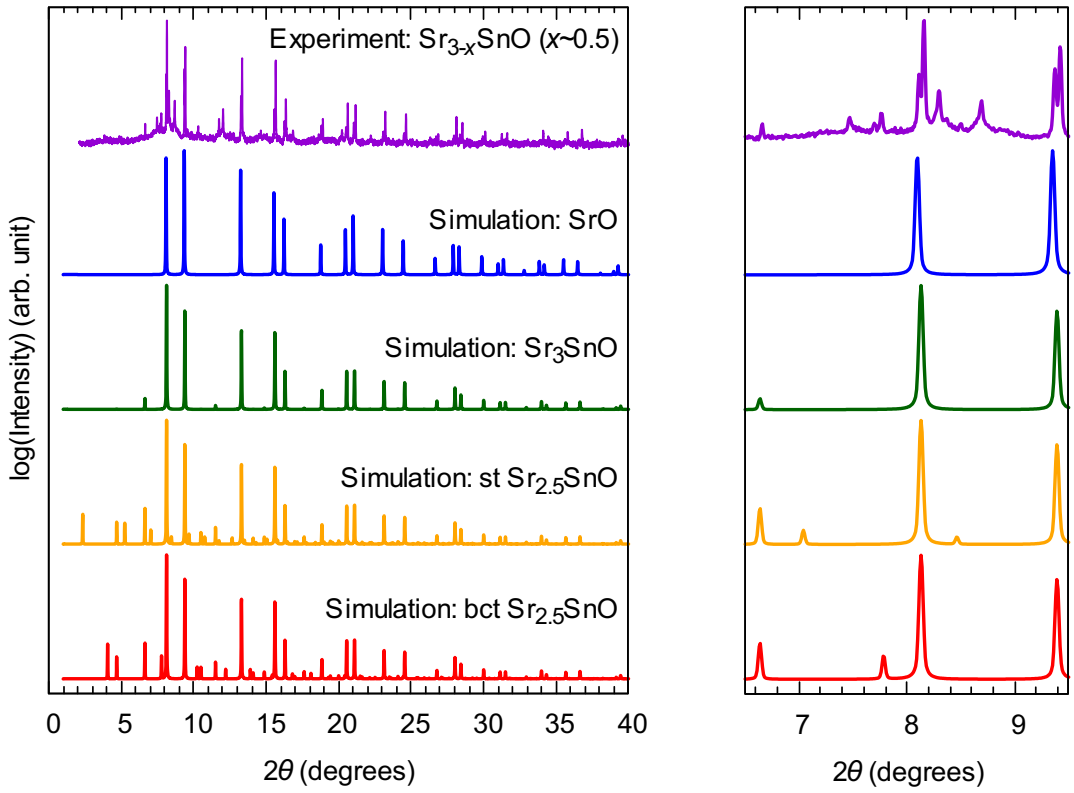

Figure 2: Observed and simulated powder X-ray diffraction spectra of $Sr_{3-x}SnO$ and SrO. The purple one is the experimental data for the superconductive $Sr_{3-x}SnO$ ($x \sim 0.5; T_c \sim 5.2$ K) measured at 30 K and at SPring-8. The blue, green, yellow, and red ones are the simulated patterns for SrO, Sr_3SnO, the simple-tetragonal (st) $Sr_{3-x}SnO$ ($x = 0.5$) shown in Fig. 1(b), and the body-centered-tetragonal (bct) $Sr_{3-x}SnO$ ($x = 0.5$) shown in Fig. 1(c), respectively. The spectra were calculated using VESTA [2].

centered tetragonal $Sr_{3-x}SnO$ [Fig. 1(c)] and $10\times10\times5$ for the simple-tetragonal $Sr_{3-x}SnO$ [Fig. 1(b)]. Figures 1(e) and (f) show the Brillouin zones of the simple and body-centered tetragonal lattices and k paths used for the band-structure plots.

When using AkaiKKR, the muffin-tin radius R of each atom was set to $R_{\rm Sr} = R_{\rm Sn} = R_{\rm O} = a/4$, where a is the lattice constant. We set the small imaginary part of the energy $E_{\rm delt} = 0.0003$ Ry and separation energy between the valence and core states $E_{\rm width} = 1.9$ Ry. A k mesh of $8 \times 8 \times 8$ was used for the calculation of Sr_3SnO and $Sr_{3-x}SnO$. For the calculation of $Sr_{3-x}SnO$, we used the coherent potential approximation [19, 20], which allows us to calculate randomly disordered systems.

3. Results and Discussion

The obtained powder X-ray-diffraction spectrum of the superconductive $Sr_{3-x}SnO$ ($x \sim 0.5$) sample is shown in Fig. 2, together with simulations for SrO, stoichiometric Sr_3SnO, and two hypothetical $Sr_{3-x}SnO$ structures. The experimental pattern basically matches with the simulation for Sr_3SnO. Nevertheless, the experimental pattern exhibits clear phase splitting evidenced by the double peaks shown in the right panel. We consider that the minor phase is SrO (face-centered cubic, space group $Fm\bar{3}m$, No. 225, O_h^5) for the following two reasons. First, the peak at 6.6° does not split. Because only Sr_3SnO has a peak at 6.6°, this absence of the splitting means that there is only one Sr_3SnO phase in the sample. Second, while the peak around 8.2° has larger intensity than the one around 9.4° in the simulation for Sr_3SnO, the peak at 9.4° is higher in SrO. The major and minor phases in the observed spectrum have the same tendency as Sr_3SnO and SrO, respectively. These data suggest that the sample consists of $Sr_{3-x}SnO$ as the major phase and SrO as a minor one. From the positions of some sharp peaks, the cell parameters a of the major and minor phases were evaluated to be 0.512152 ± 0.000010 nm and 0.51495 ± 0.00004 nm, respectively, where the errors represent the standard errors of the least square fittings. These values are consistent with the reported cell parameters $a = 0.51394$ nm [11] for Sr_3SnO and $a = 0.51615$ nm [21] for SrO. No clear peaks originating from the superstructures were observed below $2\theta = 7°$, suggesting that the strontium deficiencies are randomly distributed. Although in the high angles there are some peaks which coincide with the superlattice peaks, we consider that they are attributable to impurities.

Figures 3 (a) and (b) show the energy bands of Sr_3SnO calculated using WIEN2k and AkaiKKR, respectively, without spin-orbit coupling. Two programs produce similar band structures with Dirac cones along the $\Gamma - X$ line. It is noticeable that the bands are metallic because of the valence bands exceeding the Fermi energy at the Γ point. Figures 3(c) and (d) are the energy dispersions calculated with WIEN2k and AkaiKKR, respectively, with spin-orbit coupling. Although the overall shapes of the bands are roughly consistent between the two packages, there are some detailed differences. First, while WIEN2k shows a semiconducting band structure with a slight gap of 0.039 eV, AkaiKKR retains a metallic structure. According to the tight-binding model [5] for Ca_3PbO, another antiperovskite oxide with the band inversion, the four states (corresponding to the two lines due to the time-reversal symmetry) contributing to the valence bands just below the Fermi energy are the states with the total angular momentum $J = 3/2$ of Sn-5p orbitals. Among the $J = 3/2$ states, only the $J_z = \pm1/2$ states are energetically lowered by the band repulsion with the conduction bands while the $J_z = \pm3/2$ states form the Dirac cone because of the suppression of the repulsion by the crystalline and orbital symmetries. This band repulsion between the $J_z = \pm1/2$ states and the conduction bands, or the effect of the spin-orbit interaction of tin, seems smaller in AkaiKKR than in WIEN2k, resulting in the metallic band structure in the latter. The discrepancy likely originates from the two programs using different calculation methods. Since nonmetallic temperature dependence of the resistivity is experimentally observed for stoichiometric Sr_3SnO [8, 10, 13], the band structure obtained by WIEN2k must be closer to the actual band. Second, the band structure by WIEN2k has two four-fold degeneracies above and below the Fermi energy at the Γ point. On the other hand, AkaiKKR lifts the one above the Fermi energy. This may be because AkaiKKR takes into account only the Bravais lattices while WIEN2k considers all the symmetries in the space groups.

Figure 4 shows the dispersion relations of $Sr_{3-x}SnO$ calculated using WIEN2k and AkaiKKR with spin-orbit interaction. We adopted the coherent potential approximation in Fig. 4(c) to take into account the random deficiency observed in the X-ray diffraction measurement. In all calculations, reflecting the hole doping by the strontium deficiency, the Fermi energy is located at around 0.8 eV below the trace of the Dirac cone. Though the two programs predict different amount of repulsion between the valence and conduction bands, such a difference around the original Fermi energy of Sr_3SnO does not affect much to the properties of heavily doped $Sr_{3-x}SnO$ ($x \sim 0.5$). This amount of lowering of the Fermi energy is consistent with the expected value from the rigid-band shift of Fig. 3. In fact, considering the number of the carriers, the rigid-band shift of Figs. 3(c) and (d) give Fermi energies of -0.9 eV and -0.8 eV for $Sr_{3-x}SnO$ with $x = 0.5$, respectively. Since the band inversion in Sr_3SnO occurs down to about -0.06 eV in Fig. 3(c) and to -0.16 eV in Fig. 3(d), p-d mixing necessary to the topological crystalline superconductivity is considered to be tiny in the samples with $x \sim 0.5$. Naively, for the topological crystalline superconductivity, hole doping shifting the Fermi energy by 0.06 eV with respect to Fig. 3(c) or by 0.16 eV with respect to Fig. 3(d), which corresponds to $x = 0.0002$ or $x = 0.01$ assuming the rigid-band shift, will be favorable.

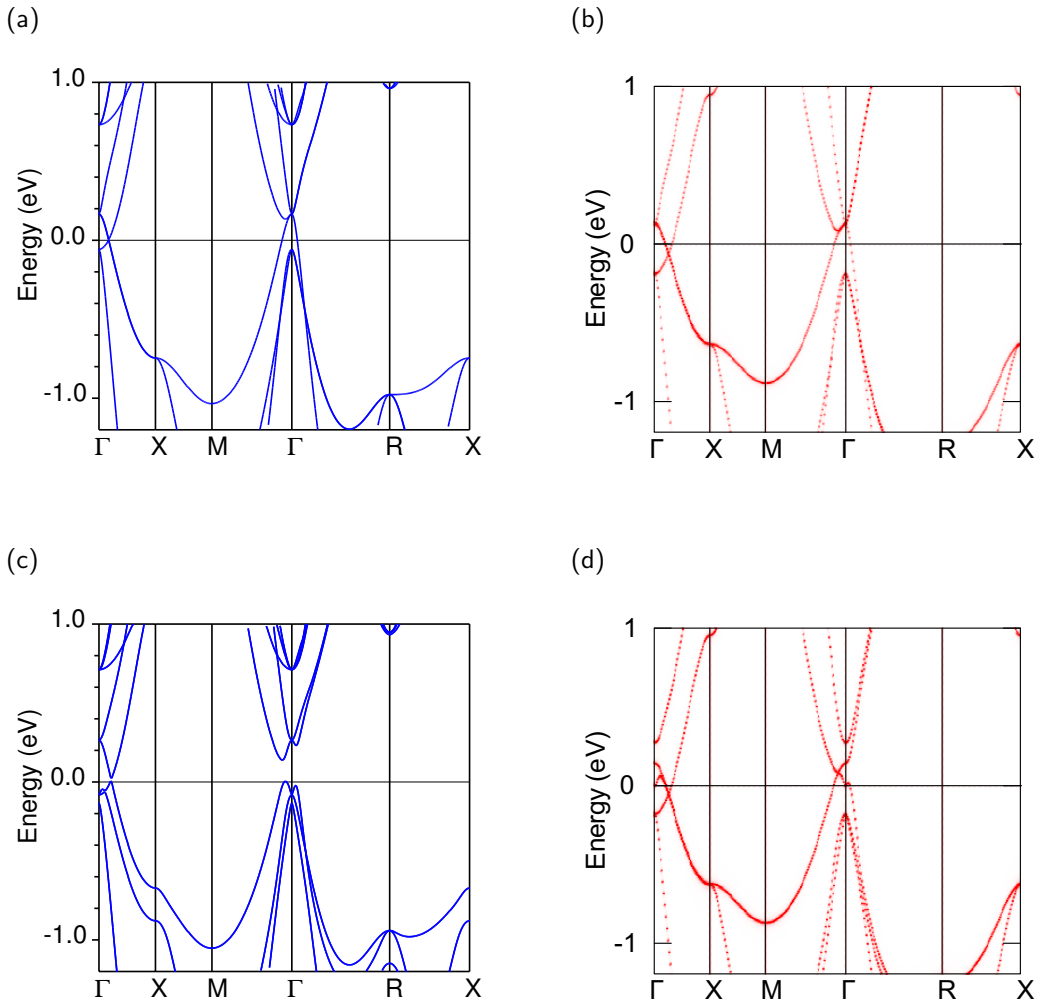

Figure 3: (a, c) Band structures of Sr_3SnO calculated using WIEN2k [14] excluding and including spin-orbit interactions, respectively. (b, d) Bloch spectral functions of Sr_3SnO calculated using AkaiKKR (Machikaneyama) [15] excluding and including spin-orbit interactions, respectively.

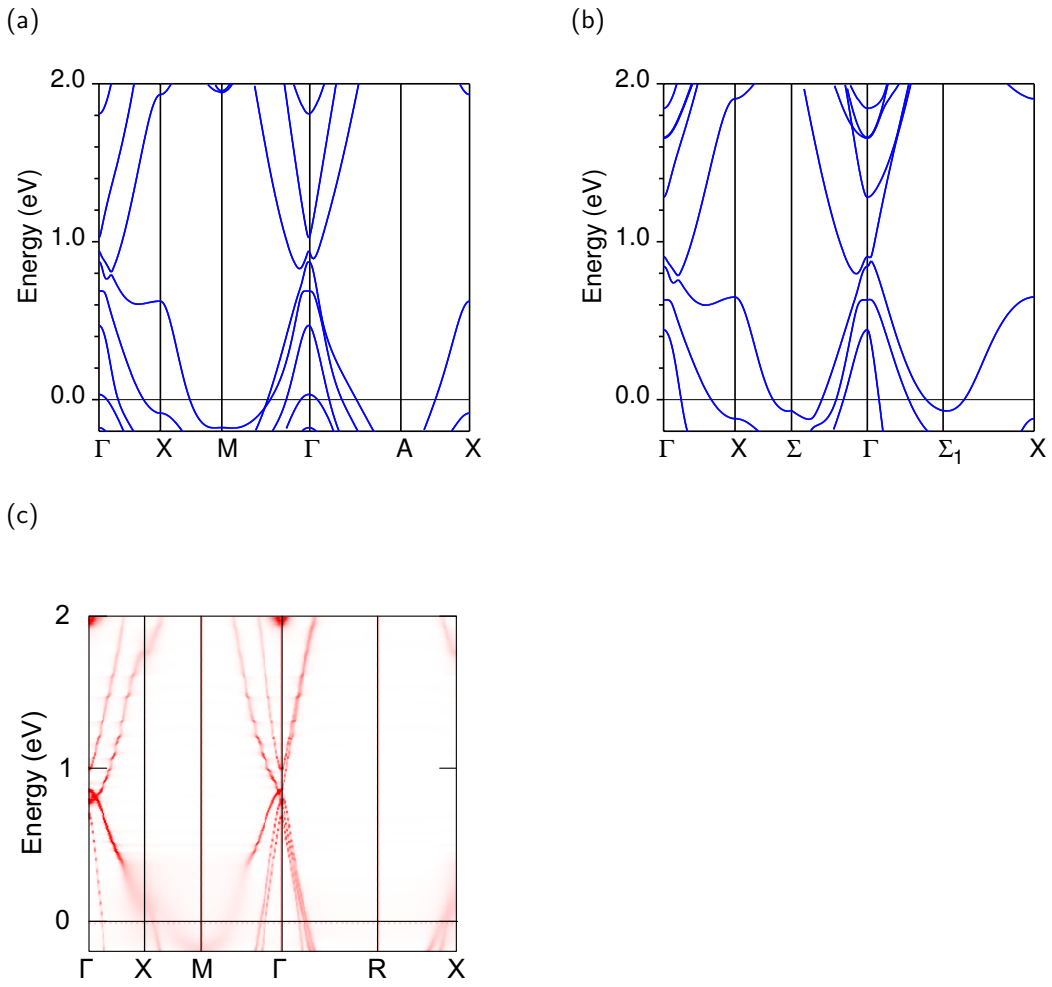

Figure 4: Band structures of $Sr_{3-x}SnO$ ($x \sim 0.5$) calculated using (a, b) WIEN2k [14] and (c) AkaiKKR (Machikaneyama) [15]. The panels (a) and (b) correspond to the hypothetical deficient structures presented in Figs. 1(b) and (c), respectively. (c) is the Bloch spectral function calculated using the coherent potential approximation [19, 20] with a strontium deficiency of 17% ($x = 0.51$). In the blurred region, states have finite lifetime because of the scattering by the random deficiency.

4. Conclusion

We synthesized superconductive $Sr_{3-x}SnO$ ($x \sim 0.5$) and observed no evidence of the superstructure related to the strontium deficiency in the X-ray diffraction spectrum. Using the supercell method and the coherent potential approximation, we calculated the band structures of $Sr_{3-x}SnO$ ($x \sim 0.5$) and found that the Fermi energy is lowered by about 0.8 eV from that of Sr_3SnO because of the hole doping. For the topological crystalline superconductivity predicted in the mixed region of the valence p and conduction d bands, hole doping smaller than $x = 0.01$ will be favorable.

Acknowledgements

We thank Yukio Tanaka for various discussions. We also acknowledge Hitoshi Gomi and Computational Materials Design Workshop for the instruction in AkaiKKR (Machikaneyama). This work was supported by the JSPS KAKENHI Nos. JP15H05851, JP15H05852, JP15H05853 and JP15H05855 (Topological Materials Science) as well as by Izumi Science and Technology Foundation (Grant No. H28-J-146). AI is supported by Japan Society for the Promotion of Science (JSPS) as JSPS Research Fellow.

References

[1] A. Widera, H. Schafer, Übergangsformen zwischen zintlphasen und echten salzen: Die verbindungen A_3BO (MIT A = Ca, Sr, Ba und B = Sn, Pb), Mater. Res. Bull. 15 (12) (1980) 1805–1809. doi:http://dx.doi.org/10.1016/0025-5408(80)90200-7.

[2] K. Momma, F. Izumi, VESTA 3 for three-dimensional visualization of crystal, volumetric and morphology data, J. Appl. Crystallogr. 44 (6) (2011) 1272–1276. doi:10.1107/S0021889811038970.

[3] A. Kokalj, Computer graphics and graphical user interfaces as tools in simulations of matter at the atomic scale, in: Proceedings of the Symposium on Software Development for Process and Materials Design, Vol. 28, 2003, pp. 155–168. doi:https://doi.org/10.1016/S0927-0256(03)00104-6.

[4] M. Klintenberg, J. T. Haraldsen, A. V. Balatsky, Computational Search for Strong Topological Insulators: An Exercise in Data Mining and Electronic Structure, Appl. Phys. Res. 6 (4) (2014) 31–41. doi:10.5539/apr.v6n4p31.

[5] T. Kariyado, M. Ogata, Three-Dimensional Dirac Electrons at the Fermi Energy in Cubic Inverse Perovskites: Ca_3PbO and Its Family, J. Phys. Soc. Jpn. 80 (8) (2011) 083704. doi:10.1143/JPSJ.80.083704.

[6] T. Kariyado, M. Ogata, Low-Energy Effective Hamiltonian and the Surface States of Ca_3PbO, Journal of the Physical Society of Japan 81 (6) (2012) 064701. doi:10.1143/JPSJ.81.064701.

[7] T. H. Hsieh, J. Liu, L. Fu, Topological crystalline insulators and Dirac octets in antiperovskites, Phys. Rev. B 90 (2014) 081112. doi:10.1103/PhysRevB.90.081112.

[8] Y. F. Lee, F. Wu, R. Kumar, F. Hunte, J. Schwartz, J. Narayan, Epitaxial integration of dilute magnetic semiconductor Sr_3SnO with Si (001), Appl. Phys. Lett. 103 (11) (2013) 112101. doi:10.1063/1.4820770.

[9] Y. Lee, F. Wu, J. Narayan, J. Schwartz, Oxygen vacancy enhanced room-temperature ferromagnetism in Sr_3SnO/c-YSZ/Si (001) heterostructures, MRS Communications 4 (1) (2014) 7–13. doi:10.1557/mrc.2014.4.

[10] Y. F. Lee, J. Narayan, J. Schwartz, Tunable electronic structure in dilute magnetic semiconductor Sr_3SnO/c-YSZ/Si (001) epitaxial heterostructures, J. Appl. Phys. 116 (16) (2014) 164903. doi:10.1063/1.4899438.

[11] J. Nuss, C. Mühle, K. Hayama, V. Abdolazimi, H. Takagi, Tilting structures in *inverse* perovskites, M_3TtO (M = Ca, Sr, Ba, Eu; Tt = Si, Ge, Sn, Pb), Acta Cryst. B 71 (3) (2015) 300–312. doi:10.1107/S2052520615006150.

[12] Y. Okamoto, A. Sakamaki, K. Takenaka, Thermoelectric properties of antiperovskite calcium oxides Ca_3PbO and Ca_3SnO, J. Appl. Phys. 119 (20) (2016) 205106. doi:10.1063/1.4952393.

[13] M. Oudah, A. Ikeda, J. N. Hausmann, S. Yonezawa, T. Fukumoto, S. Kobayashi, M. Sato, Y. Maeno, Superconductivity in the antiperovskite Dirac-metal oxide $Sr_{3-x}SnO$, Nat. Commun. 7 (2016) 13617. doi:10.1038/ncomms13617.

[14] P. Blaha, K. Schwarz, G. Madsen, D. Kvasnicka, J. Luitz, WIEN2k, An Augmented Plane Wave Plus Local Orbital Program for Calculating Crystal Properties, Vienna University of Technology Institute of Materials Chemistry, Vienna, Austria (Dec 2016).
URL http://susi.theochem.tuwien.ac.at/index.html

[15] K. Sato, M. Ogura, H. Akai, Band structure calculation using KKR-Green's function method (Aug 2008).
URL http://kkr.issp.u-tokyo.ac.jp/

[16] J. Korringa, On the calculation of the energy of a Bloch wave in a metal, Physica 13 (6) (1947) 392–400. doi:10.1016/0031-8914(47)90013-X.

[17] W. Kohn, N. Rostoker, Solution of the Schrödinger Equation in Periodic Lattices with an Application to Metallic Lithium, Phys. Rev. 94 (1954) 1111–1120. doi:10.1103/PhysRev.94.1111.

[18] J. P. Perdew, K. Burke, M. Ernzerhof, Generalized Gradient Approximation Made Simple, Phys. Rev. Lett. 77 (1996) 3865–3868. doi:10.1103/PhysRevLett.77.3865.

[19] H. Shiba, A Reformulation of the Coherent Potential Approximation and Its Applications, Progress of Theoretical Physics 46 (1) (1971) 77. doi:10.1143/PTP.46.77.

[20] P. Soven, Application of the Coherent Potential Approximation to a System of Muffin-Tin Potentials, Phys. Rev. B 2 (1970) 4715–4722. doi:10.1103/PhysRevB.2.4715.

[21] J. Bashir, R. T. A. Khan, N. M. Butt, G. Heger, Thermal atomic displacement parameters of SrO, Powder Diffraction 17 (3) (2002) 222–224. doi:10.1154/1.1490370.